Available online at www.sciencedirect.com
SCIENCE DIRECT®
Journal of Computational Physics 188 (2003) 296–317
JOURNAL OF COMPUTATIONAL PHYSICS
www.elsevier.com/locate/jcp

Perturbation-based moment equation approach for flow in heterogeneous porous media: applicability range and analysis of high-order terms

Liyong Li [a], Hamdi A. Tchelepi [a,*], Dongxiao Zhang [b]

[a] *ChevronTexaco E&P Technology Company, San Ramon, CA 94583, USA*
[b] *Hydrology, Geochemistry, and Geology Group MS T003, Los Alamos National Laboratory, Los Alamos, NM 87545, USA*

Received 9 September 2002; received in revised form 30 January 2003; accepted 7 March 2003

Abstract

We present detailed comparisons between high-resolution Monte Carlo simulation (MCS) and low-order numerical solutions of stochastic moment equations (SMEs) for the first and second statistical moments of pressure. The objective is to quantify the difference between the predictions obtained from MCS and SME. Natural formations with high permeability variability and large spatial correlation scales are of special interest for underground resources (e.g. oil and water). Consequently, we focus on such formations. We investigated fields with variance of log-permeability, σ_Y^2, from 0.1 to 3.0 and correlation scales (normalized by domain length) of 0.05 to 0.5. In order to avoid issues related to statistical convergence and resolution level, we used 9000 highly resolved realizations of permeability for MCS. We derive exact discrete forms of the statistical moment equations. Formulations based on equations written explicitly in terms of permeability (K-based) and log-transformed permeability (Y-based) are considered. The discrete forms are applicable to systems of arbitrary variance and correlation scales. However, equations governing a particular statistical moment depend on higher moments. Thus, while the moment equations are exact, they are not closed. In particular, the discrete form of the second moment of pressure includes two triplet terms that involve log-permeability (or permeability) and pressure. We combined MCS computations with full discrete SME equations to quantify the importance of the various terms that make up the moment equations. We show that second-moment solutions obtained using a low-order Y-based SME formulation are significantly better than those from K-based formulations, especially when $\sigma_Y^2 > 1$. As a result, Y-based formulations are preferred. The two triplet terms are complex functions of the variance level and correlation length. The importance (contribution) of these triplet terms increases dramatically as σ_Y^2 increases above one. We also show that one of the triplet terms is much more important than the other. When comparing K-based MCS with Y-based SME, model differences must be taken into consideration. These differences (model errors) are due to embedded assumptions and differences in implementing the discrete forms of the equations.

Keywords: Stochastic equations; Uncertainty analysis; Statistical moments; Monte Carlo simulation; Heterogeneous porous media; Reservoir simulation; Groundwater flow

* Corresponding author. Tel.: +1-925-842-6390; fax: +1-925-842-2156.
E-mail address: HTCH@chevrontexacon.com (H.A. Tchelepi).

0021-9991/03/$ - see front matter
doi:10.1016/S0021-9991(03)00186-4

1. Introduction

Predictions of flow and transport in natural porous media are used to manage valuable subsurface resources including water aquifers and oil reservoirs. The predictions are usually made, however, in the presence of a great deal of uncertainty due to (1) sparsity of available data and (2) the observed complex spatial variability and correlation structures of formation properties, such as permeability. A probabilistic, or stochastic, framework is employed to deal with the uncertainty brought about by incomplete knowledge of the reservoir properties. Stochastic models of reservoir description, which honor available data, are common practice. However, deterministic mathematical formulations that describe the flow and transport continue to serve as the basis for reservoir flow simulators. Monte Carlo simulation (MCS) is the primary tool used in the oil industry to quantify the uncertainty in the flow response due to uncertainty in the reservoir description. In MCS, the statistical moments are computed from the results of multiple flow simulations, one per equiprobable realization of the reservoir description.

Subsurface hydrologists, on the other hand, have developed stochastic moment methods that incorporate the probabilistic nature of the formation properties, permeability for example, into the governing equations of flow and transport in heterogeneous aquifers. These stochastic moment equation (SME) methods offer an elegant and direct approach for not only making predictions of flow and transport in porous formations but also quantifying the uncertainty associated with such predictions. Formally, the validity range of these perturbation-based low-order stochastic moment equation (LOSME) methods is limited to small values of the expansion parameter, usually the standard deviation of log-permeability, $\sigma_{\ln K}$, and small correlation scales [7,9,16,30]. Notwithstanding these restrictions, the broad class of LOSME approaches represents a school of thought that is widely recognized and used. Examples include [6,8,9,11,15–18,23,26,30], among others.

Surveys of natural formations indicate that the level of variability and spatial correlation scales of permeability span a wide range [9,10,14,16,22]. It is clear from these surveys and others that high levels of permeability variability (i.e. $\sigma^2_{\ln K} > 1$) are common in practice. Moreover, large correlation scales exist in many aquifer and reservoir systems. Thus, from a practical view, it is important to be able to predict the behavior of natural formations that exhibit high variability and long correlation scales.

Higher-order terms are dropped in the process of deriving first- and second-order SME approximations. As the variance and correlation scale of permeability increase, one expects the high-order terms to play a more significant role. For example, Hassan et al. [21] found that triplet terms in the moment equations of transport can have a significant impact on the computed response even in the case where the mean flow is uniform and $\sigma^2_{\ln K}$ is close to unity. On the other hand, Guadagnini and Neuman [19,20] found that numerical solutions of the first and second moments of pressure obtained by first-order (in $\sigma^2_{\ln K}$) approximations show remarkable agreement with MCS even for strongly heterogeneous formations. In their study, they considered systems with $\sigma^2_{\ln K}$ as large as four and very long correlation scales of the permeability. Zhang and Winter [31] found similar agreement between low-order approximations and MCS results.

The central question we tackle here is how well do these LOSME methods predict the flow behavior in the parameter space of practical interest. In particular, we study the statistical moments of pressure for incompressible flow in two dimensions. Similar treatment for the transport problem in strongly heterogeneous formations will be addressed later. Our approach is based on comparison of SME solutions with high-resolution MCS. A large set of high-resolution MCS was constructed. The Monte Carlo results serve both as reference and a repository of data that can be used to analyze the complex character of the obtained responses. We use two different forms of the flow equation as a starting point. One form is based on the permeability, K, the other is based on log-transformed permeability, $Y = \ln K$. For each form, we derive the exact discrete equations of the pressure moments, which are valid for arbitrary variability levels and correlation scales. The motivation for analyzing two different equation forms is discussed later. With the help of MCS, all the terms that appear in the exact discrete moment equations, including the terms that are

dropped in LOSME formulations, can be reconstructed. We map out the behavior of the statistical moments of pressure for a wide range of the parameter space. We consider systems with a variance of log-permeability, σ_Y^2, from 0.5 to 3.0 and correlation length (normalized by domain length) from 0.05 to 0.5. We also present detailed analysis of the character and magnitude of the errors that contribute to the discrepancy between LOSME solutions and MCS results. We find that the discrepancy is mainly due to the truncation of high-order terms in the process of developing low-order, perturbation-based statistical moment approximations. For our problem, the important missing terms are two triplets that are complex functions of mixed third moments involving pressure and permeability. We also find that details of the numerical schemes employed can have a significant impact on the computations.

The paper is organized as follows. First, we develop full discrete forms of the equations governing the first two moments of pressure. These equations are valid for arbitrary variance and correlation scales. Next, we map out the detailed behavior of the statistical moments of flow-related quantities using high-resolution MCS. The focus here is on the second moment of the dependent variable, pressure. Second moments provide a measure of predictive reliability, which is a key motivation for resorting to SME methods. We then compare SME with MCS to quantify the range of applicability of SME approaches for the flow problem under investigation. By combining the full discrete form of the moment equations with results from MCS, we isolate and systematically quantify the impact of high-order terms that are usually dropped in the process of developing low-order, perturbation-based, SME approaches.

2. Governing equations

We consider the case of incompressible flow in a heterogeneous porous medium. From the continuity equation and Darcy's law, we write the equation governing the pressure distribution in the domain as

$$\frac{\partial}{\partial x}\left[K(x,y)\frac{\partial P(x,y)}{\partial x}\right]+\frac{\partial}{\partial y}\left[K(x,y)\frac{\partial P(x,y)}{\partial y}\right]=0, \tag{1}$$

where $K(x,y)$ denotes the spatially variable permeability field and $P(x,y)$ is pressure. The permeability is assumed to be a random space function, and by Eq. (1) so is the pressure. Expanding the derivatives of Eq. (1) and defining $Y(x,y)=\ln K(x,y)$, we obtain a pressure equation in terms of log-permeability

$$\frac{\partial^2 P(x,y)}{\partial x^2}+\frac{\partial^2 P(x,y)}{\partial y^2}+\frac{\partial Y(x,y)}{\partial x}\frac{\partial P(x,y)}{\partial x}+\frac{\partial Y(x,y)}{\partial y}\frac{\partial P(x,y)}{\partial y}=0. \tag{2}$$

We refer to Eqs. (1) and (2) as the K-based and Y-based equations for pressure. We may use either equation to perform MCS or derive SMEs. Traditionally, Eq. (2) is used to develop moment equations and Eq. (1) is employed in Monte Carlo simulation [3,4,20,21,32].

We use MCS to study the statistical moments of pressure when permeability variability is the source of uncertainty. In MCS, the statistical moments are obtained using an ensemble of solutions, each of which is obtained from a single highly resolved realization of the permeability distribution. Using a random field generator, such as GSLIB [12] and HydroGen [5], realizations of the permeability field are generated such that they share a common correlation structure and variability level. The appropriate level of resolution for the generated realizations is an important question. In general terms, the discretization requirements are dictated by the characteristics of the permeability field as well as the flow process under study [1,21]. In fact, the resolution requirements depend on the particular variable (e.g., pressure, velocity, production rate) under study as well as the order of the statistical moment of interest [27]. We confine the discussion here to the simple setting of uniform mean flow

$$\frac{\partial P(x,y)}{\partial y} = 0, y = 0, L, \quad P(0,y) = P_0, P(L,y) = P_1, \tag{3}$$

where L is domain length, and P_0 and P_1 are the fixed inlet and outlet pressures. This simple setting allows us to compare our findings with previous work. We also performed an extensive study of settings where the mean flow is non-uniform due to the presence of wells and no-flow boundaries. That analysis is deferred to a subsequent paper. Here, we note that while the behaviors are more complex when the mean flow is non-uniform, the fundamental mechanisms at work are the same as those in the mean uniform flow case.

3. Numerical implementation

3.1. K-Based pressure equation

To solve Eq. (1) numerically, we employ a point-distributed grid. The domain is discretized using N_i and N_j nodes in the respective x and y directions $x = x(i)$ and $y = y(j)$, where i and j are $[1, 2, 3, \ldots, N_i]$ and $[1, 2, 3, \ldots, N_j]$. The total number of nodes is $M = N_i \times N_j$.

Using a central finite-difference approximation on uniformly spaced grid, we have

$$\begin{aligned}
\frac{\partial}{\partial x}\left(K\frac{\partial P}{\partial x}\right)_{i,j} &= \frac{1}{\Delta x^2}\left[K_{i+\frac{1}{2},j}(P_{i+1,j} - P_{i,j}) - K_{i-\frac{1}{2},j}(P_{i,j} - P_{i-1,j})\right], \\
\frac{\partial}{\partial y}\left(K\frac{\partial P}{\partial y}\right)_{i,j} &= \frac{1}{\Delta y^2}\left[K_{i,j+\frac{1}{2}}(P_{i,j+1} - P_{i,j}) - K_{i,j-\frac{1}{2}}(P_{i,j} - P_{i,j-1})\right],
\end{aligned} \tag{4}$$

where $K_{i+\frac{1}{2},j}$, $K_{i,j+\frac{1}{2}}$, $K_{i-\frac{1}{2},j}$, and $K_{i,j-\frac{1}{2}}$ are interface permeabilities between nodes i and $i+1$, j and $j+1$, i and $i-1$, and j and $j-1$, respectively. Fig. 1 shows the locations of the variables on the grid. From a control-volume discretization perspective, the gridblock permeability is defined at the cell center. The interface value, $K_{i+\frac{1}{2},j}$ for example, is taken as the harmonic average of the two permeability values defined at the cell centers, or control volumes, i and $i+1$. The harmonic average preserves continuity of pressure and flux at the interface [2]. Preserving flux continuity is necessary for local conservation and can have important implications when the gridblocks (control volumes) are large and/or the discrete representation of permeability is highly discontinuous. For interior nodes, or gridblocks, Eq. (1) can be expressed as

$$K_{i+\frac{1}{2},j}P_{i+1,j} + K_{i-\frac{1}{2},j}P_{i-1,j} + K_{i,j+\frac{1}{2}}P_{i,j+1} + K_{i,j-\frac{1}{2}}P_{i,j-1} - (K_{i+\frac{1}{2},j} + K_{i-\frac{1}{2},j} + K_{i,j+\frac{1}{2}} + K_{i,j-\frac{1}{2}})P_{i,j} = 0. \tag{5}$$

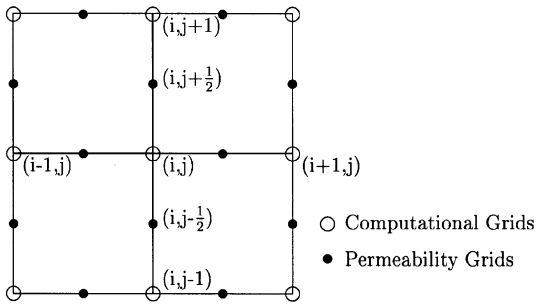

Fig. 1. The computational and permeability grids in the domain.

Application of reflection at the no-flow boundary, $y = 0$ for example, yields

$$K_{i+\frac{1}{2},j}P_{i+1,j} + K_{i-\frac{1}{2},j}P_{i-1,j} + 2K_{i,j+\frac{1}{2}}P_{i,j+1} - \left(K_{i+\frac{1}{2},j} + K_{i-\frac{1}{2},j} + 2K_{i,j+\frac{1}{2}}\right)P_{i,j} = 0. \tag{6}$$

We can write similar equations for the other no-flow boundaries. Using matrix notation, we write

$$\mathbf{KP} = 0. \tag{7}$$

Eq. (7) is the discrete representation of Eq. (1). It is usually referred to as the pressure equation in reservoir engineering, and the space-state equation in hydrology [13]. For our structured two-dimensional grid, $\mathbf{K}$ is a banded $M \times M$ permeability (transmissibility) matrix and $\mathbf{P}$ is the pressure vector of M elements. The boundary conditions are usually absorbed into the coefficient matrix; internal sources and sinks may appear as source terms on the right-hand side of Eq. (7).

3.2. K-Based Monte Carlo simulation

The steps for MCS are: (1) generate a large number of permeability realizations, (2) solve Eq. (7) for each realization, and (3) perform statistical post-processing of the quantities of interest. Here, we assume that permeability is lognormally distributed and is second-order stationary in space, such that the mean log permeability is constant and its covariance depends on the relative distance of two points rather than their actual locations. These assumptions are made here for convenience; our computational tools accommodate non-stationary correlation structures and complex domain geometry. The permeability fields were generated using the HydroGen [5] and SGSIM of GSLIB [12] software packages. The range of parameters investigated in this study spans a variance of log-permeability, $\sigma^2_{\ln K}$, from 0.1 to 3 and integral scales (normalized by domain size) from 0.05 to 0.5. Table 1 lists the details of the cases studied here.

With MCS, an important question is statistical convergence of the computed moments. That is, how many realizations are necessary. We tested the statistical convergence of the moments not only of permeability but also of the dependent variable, pressure. Fig. 2 shows the convergence behavior of the sample

Table 1
Input parameters for different MC simulation cases

Parameter	Case 1	Case 2	Case 3	Case 4	Case 5
σ^2_Y	0.1	0.1	0.1	0.1	
$\frac{\lambda_Y}{L}$	$\frac{0.25}{5.} = 0.05$	$\frac{0.5}{5.} = 0.1$	$\frac{1.}{5.} = 0.2$	$\frac{2.}{5.} = 0.4$	$\frac{2.5}{5.} = 0.5$
$\frac{\lambda_Y}{\Delta x}$	$\frac{0.25}{.125} = 2$	$\frac{0.5}{0.125} = 4$	$\frac{1.0}{.125} = 8$	$\frac{2.0}{.125} = 16$	$\frac{2.5}{.125} = 20$
σ^2_Y	0.25	0.25	0.25	0.25	0.25
$\frac{\lambda_Y}{L}$	$\frac{0.25}{5.} = 0.05$	$\frac{0.5}{5.} = 0.1$	$\frac{1.}{5.} = 0.2$	$\frac{2.}{5.} = 0.4$	$\frac{2.5}{5.} = 0.5$
$\frac{\lambda_Y}{\Delta x}$	$\frac{0.25}{.125} = 2$	$\frac{0.5}{0.125} = 4$	$\frac{1.0}{.125} = 8$	$\frac{2.0}{.125} = 16$	$\frac{2.5}{.125} = 20$
σ^2_Y	0.5	0.5	0.5	0.5	0.25
$\frac{\lambda_Y}{L}$	$\frac{0.25}{5.} = 0.05$	$\frac{0.5}{5.} = 0.1$	$\frac{1.}{5.} = 0.2$	$\frac{2.}{5.} = 0.4$	$\frac{2.5}{5.} = 0.5$
$\frac{\lambda_Y}{\Delta x}$	$\frac{0.25}{.125} = 2$	$\frac{0.5}{0.125} = 4$	$\frac{1.0}{.125} = 8$	$\frac{2.0}{.125} = 16$	$\frac{2.5}{.125} = 20$
σ^2_Y	1	1	1	1	1
$\frac{\lambda_Y}{L}$	$\frac{0.25}{5.} = 0.05$	$\frac{0.5}{5.} = 0.1$	$\frac{1.}{5.} = 0.2$	$\frac{2.}{5.} = 0.4$	$\frac{2.5}{5.} = 0.5$
$\frac{\lambda_Y}{\Delta x}$	$\frac{0.25}{.125} = 2$	$\frac{0.5}{0.125} = 4$	$\frac{1.0}{.125} = 8$	$\frac{2.0}{.125} = 16$	$\frac{2.5}{.125} = 20$
σ^2_Y	3	3	3	3	3
$\frac{\lambda_Y}{L}$	$\frac{0.25}{5.} = 0.05$	$\frac{0.5}{5.} = 0.1$	$\frac{1.}{5.} = 0.2$	$\frac{2.}{5.} = 0.4$	$\frac{2.5}{5.} = 0.5$
$\frac{\lambda_Y}{\Delta x}$	$\frac{0.25}{.125} = 2$	$\frac{0.5}{0.125} = 4$	$\frac{1.0}{.125} = 8$	$\frac{2.0}{.125} = 16$	$\frac{2.5}{.125} = 20$

Note. λ_Y is the correlation scale of Y; $Y = \ln K$, where K is the absolute permeability.

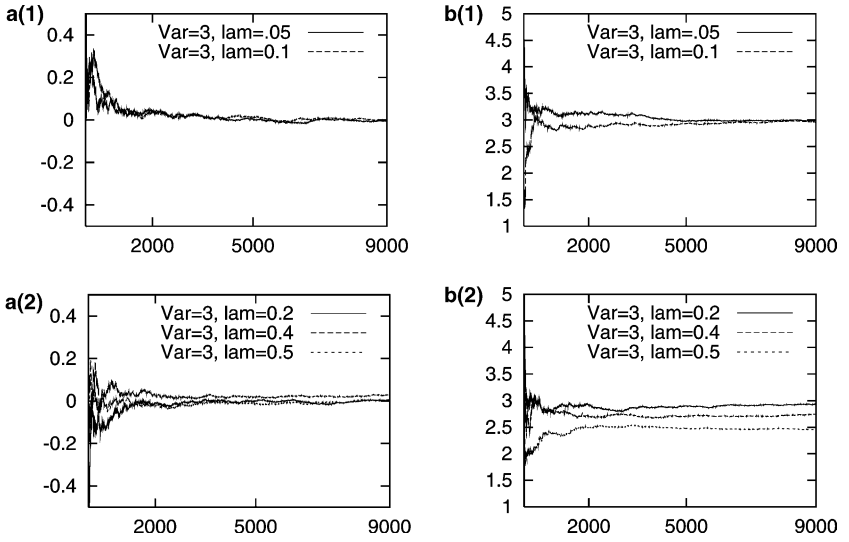

Fig. 2. The convergence of statistical moments of permeability with respect to the number of realizations where $\sigma^2_{\ln K} = 3$: (a) mean permeability; (b) permeability variance.

mean (a) and variance (b) of log-permeability as a function of the number of realizations. Fig. 2 is for the case with input $\sigma^2_{\ln K} = 3$ and a variety of correlation lengths. The sample mean and variance are reported for one point in the domain. The point is selected as follows: After 9000 realizations are generated, the sample statistics are computed and compared to the corresponding values obtained based on the first 8999 realizations; then the point with the maximum difference is marked for each quantity (mean or variance) and the sample mean or variance at that point is computed as a function of the number of realizations. As such, the grid point used to report the sample mean may be different from that for the variance. Fig. 2 shows that the sample statistics converge, or stabilize, after about 2000 realizations. The mean log-permeability converges to the input value for all cases studied. However, it is more difficult for sample variances to converge to the target input values. Fig. 2 indicates that agreement between the input and sample variance deteriorates as the correlation length (normalized by the domain size) increases. It is well known that input statistics are difficult to honor exactly for highly variable random fields with long correlation scales. To avoid issues related to this problem, we computed the statistics (mean, variance and covariances) of the generated ensemble. These statistics were then used as input for the SME simulations instead of the theoretical values.

Fig. 3 shows an example of the convergence of sample statistical moments of pressure at one point. In Fig. 3, $\sigma^2_{\ln K} = 3$ and the normalized correlation scale ranges from 0.05 to 0.5. The pressure statistics also appear to stabilize after 2000 realizations. In general, we find that for a particular variable, permeability or pressure, for example, a larger ensemble is generally needed to stabilize second moments compared with first moments. We also find that the adequate size of the ensemble grows as the variance and integral scale of permeability increase. Bellin et al. [3] used two-dimensional MCS of flow and transport in heterogeneous systems to investigate the validity of first-order moment-based theories. They studied the convergence behavior of the computed moments of both velocity and particle trajectory. They found that more than 1000 realizations are required to stabilize the moments of the ensemble, especially second moments, even for relatively mild heterogeneity. Our experience with the flow problem is consistent with their findings. The need for such large numbers of realizations to obtain reliable statistical moments, especially second moments, of pressure and other flow-related quantities is an enormous hurdle for practical use of high-resolution MCS. This does not appear to be widely recognized in the reservoir engineering community. This is

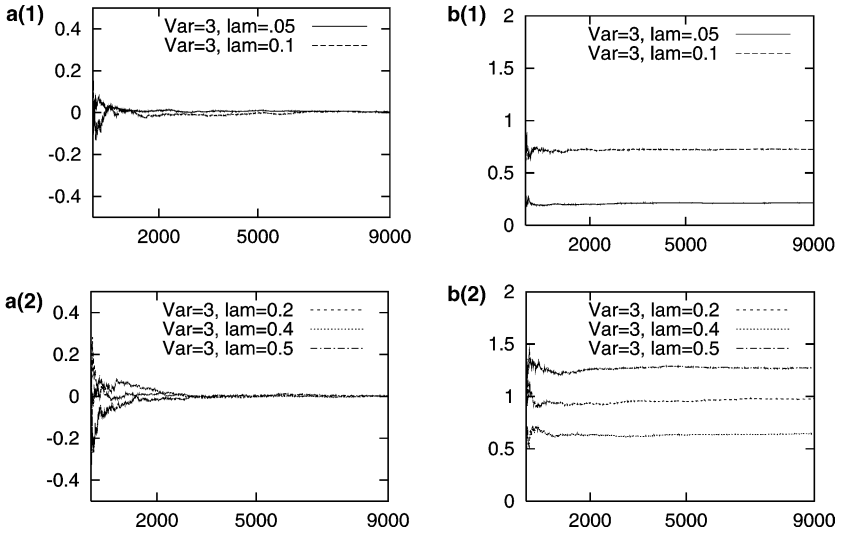

Fig. 3. The convergence of statistical moments of pressure for uniform mean flow as a function of the number of realizations when $\sigma^2_{\ln K} = 3$: (a) mean pressure; (b) pressure variance.

especially important these days because of the growing interest and use of Monte Carlo simulation for providing quantitative measures of the uncertainty associated with flow predictions.

During the course of our analysis, we developed an extensive dataset of high-resolution MCS results for flow in two-dimensional heterogeneous domains. Performing high-resolution MCS presents its own challenges; the two notable examples being (1) the appropriate resolution level and (2) size of the ensemble. However, we will not address these issues here. Our focus is on understanding the detailed characteristics of the statistical moments of flow-related quantities for heterogeneous domains with large permeability variance and long correlation scales. Thus, while 2000 realizations appear adequate for the parameter range under investigation, we employ 9000 realizations for all the cases presented in this paper. In this context, MCS is a tool that helps us map out the regions of the parameter space where low-order SME approximations are adequate, and those regions where improvements are needed.

We used the exponential covariance model to describe the correlation structure of the log-permeability field

$$C_Y(\mathbf{r}) = \sigma_Y^2 \exp\left[-\left(\frac{r_1^2}{\lambda_1^2} + \frac{r_2^2}{\lambda_2^2} \right)^{1/2} \right], \tag{8}$$

where $\mathbf{r}$ is the separation vector between two points, σ_Y^2 is the variance of log-permeability, and λ_i is the correlation (integral) scale of log-permeability in the r_i direction.

To obtain accurate numerical solutions, Hassan et al. [21] recommend a ratio of the integral (correlation) scale to the size of computational gridblock, of four, or larger. The quality of the discrete representation of the correlation structure is tested by comparing the statistical moments obtained from the ensemble with the input analytical model. Fig. 4 shows the correlation function along the lines $x = L/2$ and $y = L/2$ with respect to the reference point $x' = L/2, y' = L/2$. In order to eliminate the impact of harmonic averaging, which is usually employed to obtain an interface value that ensures flux continuity in the discrete form of the pressure equation, the interface permeability values are generated directly for the purpose of performing MCS. Thus, we make sure that the statistical moments of the

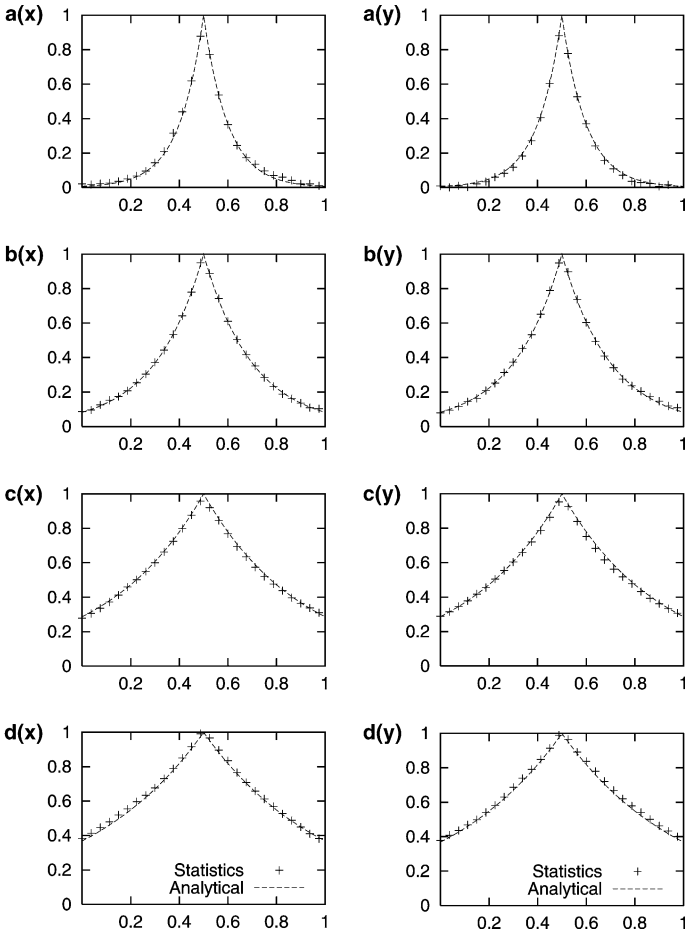

Fig. 4. A comparison of the analytical permeability correlation function, in the x and y directions, with results computed from the ensemble of realizations. The normalized integral correlation scales are: (a) 0.1, (b) 0.2, (c) 0.4, and (d) 0.5, respectively.

input permeability, especially the variance, are preserved. Refer to Fig. 1 for a schematic of the computational grid.

3.3. K-Based stochastic moment equations

In this section, we develop a discrete form of the K-based stochastic moment equations. We use Eq. (7), which is the discrete form of Eq. (1) as the starting point. For any random variable

$$\begin{aligned} K &= \langle K \rangle + K', \quad \langle K' \rangle = 0, \\ P &= \langle P \rangle + P', \quad \langle P' \rangle = 0, \end{aligned} \tag{9}$$

where $\langle\ \rangle$ represents mathematical expectation, or ensemble averaging. Substituting Eq. (9) into Eq. (7) and taking expectation gives the equation governing the mean pressure

$$\langle \mathbf{K} \rangle \langle \mathbf{P} \rangle + \langle \mathbf{K}' \mathbf{P}' \rangle = 0. \tag{10}$$

The equation for the pressure perturbations is obtained by subtracting Eq. (10) from Eq. (7)

$$\langle \mathbf{K} \rangle \mathbf{P}' + \mathbf{K}' \langle \mathbf{P} \rangle + \mathbf{K}' \mathbf{P}' - \langle \mathbf{K}' \mathbf{P}' \rangle = 0. \tag{11}$$

Multiplying Eq. (11) with P' and K' at a particular location and averaging, we obtain the following relations:

$$\begin{aligned} &\langle \mathbf{K} \rangle C_{PP} + \mathbf{C}_{\mathbf{PK}} \langle \mathbf{P} \rangle + \langle P' \mathbf{K}' \mathbf{P}' \rangle = 0, \\ &\langle \mathbf{K} \rangle C_{KP} + \mathbf{C}_{\mathbf{KK}} \langle \mathbf{P} \rangle + \langle K' \mathbf{K}' \mathbf{P}' \rangle = 0, \end{aligned} \tag{12}$$

where $\mathbf{C}_{\mathbf{KK}} = \langle K' \mathbf{K}' \rangle$ is the (input) permeability covariance matrix, $C_{PP} = \langle P' \mathbf{P}' \rangle$ is the pressure covariance vector, and $C_{KP} = \langle K' \mathbf{P}' \rangle$ is the cross-covariance vector of permeability and pressure. We choose to work with these discrete forms directly. Of course, a continuous differential form of these "exact" equations can also be derived [19,30]. The discrete forms given by Eqs. (10) and (12) are exact on the given grid in that no terms have been neglected. They are thus valid for any input permeability variance and correlation scale. However, these equations are "not closed" because equations for the second moments depend on two third (triplet) moments. One can certainly write similar equations for the third moments, which will turn out to include some mixed fourth moments. In general, the equations for the nth moments generally require knowledge of the $(n+1)$th moments. Theoretically speaking, an infinite hierarchy of equations needs to be evaluated for each moment. This is the so-called closure problem [30]. The closure problem is usually treated by approximating the nth moment in terms of lower moments. One particular approximation commonly used in low-order stochastic analysis is to simply neglect the triplet moments when evaluating second moments, which leads to

$$\begin{aligned} &\langle \mathbf{K} \rangle C_{PP} + \mathbf{C}_{\mathbf{PK}} \langle \mathbf{P} \rangle = 0, \\ &\langle \mathbf{K} \rangle C_{KP} + \mathbf{C}_{\mathbf{KK}} \langle \mathbf{P} \rangle = 0. \end{aligned} \tag{13}$$

This set of moment equations is equivalent to the first-order equations derived using the method of Adomian decomposition on the basis of a K-based representation [28,30, Section 3.9]. Since the two triplet moment terms can be computed from our extensive repository of MCS results, their contributions to the second moments can be quantified. Detailed discussion of these results is presented later. Combining the full discrete form of the SMEs with the results from MCS in this manner is a powerful method for the systematic analysis and quantification of the character, size, and relative importance of the various terms, especially those that are usually dropped in the perturbation-based SME approach.

We note that the numerical implementations of the statistical moment equations (10) and (12) are completely consistent with the implementation of Eq. (7), which is used to perform K-based MCS. We show later that complete consistency in the discrete representation and solution methods is important when MCS is used to analyze and validate low-order SME methods.

3.4. The Y-based pressure equation

We derive a discrete form of Eq. (2). Using centered differences on a point-distributed grid in two dimensions, we obtain

$$\begin{aligned} \left(\frac{\partial^2 P}{\partial x^2} \right)_{i,j} &= \frac{1}{\Delta x^2} (P_{i+1,j} - 2P_{i,j} + P_{i-1,j}), \\ \left(\frac{\partial^2 P}{\partial y^2} \right)_{i,j} &= \frac{1}{\Delta y^2} (P_{i,j+1} - 2P_{i,j} + P_{i,j-1}), \end{aligned} \tag{14}$$

and we express terms involving first derivatives as

$$\left(\frac{\partial Y}{\partial x}\frac{\partial P}{\partial x}\right)_{i,j} = \frac{1}{2\Delta x^2}\left(Y_{i+\frac{1}{2},j} - Y_{i-\frac{1}{2},j}\right)\left(P_{i+1,j} - P_{i-1,j}\right),$$
$$\left(\frac{\partial Y}{\partial y}\frac{\partial P}{\partial y}\right)_{i,j} = \frac{1}{2\Delta y^2}\left(Y_{i,j+\frac{1}{2}} - Y_{i,j-\frac{1}{2}}\right)\left(P_{i,j+1} - P_{i,j-1}\right), \tag{15}$$

where, consistent with use of interface K values, interface Y values are used.

For interior nodes, the discrete form of Eq. (2) is

$$(P_{i+1,j} + P_{i-1,j} + P_{i,j+1} + P_{i,j-1} - 4P_{i,j}) + \frac{1}{2}\left(Y_{i+\frac{1}{2},j} - Y_{i-\frac{1}{2},j}\right)(P_{i+1,j} - P_{i-1,j}) + \frac{1}{2}\left(Y_{i,j+\frac{1}{2}} - Y_{i,j-\frac{1}{2}}\right)(P_{i,j+1} - P_{i,j-1}) = 0. \tag{16}$$

At a no-flow boundary such as at $y = 0$, the pressure equation is

$$(P_{i+1,j} + P_{i-1,j} + 2P_{i,j+1} - 4P_{i,j}) + \frac{1}{2}\left(Y_{i+\frac{1}{2},j} - Y_{i-\frac{1}{2},j}\right)(P_{i+1,j} - P_{i-1,j}) = 0 \tag{17}$$

since $P_{i,j+1} - P_{i,j-1} = 0$. A compact discrete representation of the Y-based pressure equation, Eq. (2), is

$$\mathbf{YP} = 0, \tag{18}$$

where $\mathbf{Y}$ is a banded $M \times M$ log-permeability matrix.

3.5. Y-Based Monte Carlo simulation

It is common practice to use K-based MCS to validate Y-based SME approaches. One reason for this is that the numerical tools for solving the governing deterministic, single-realization, equations have been traditionally developed in terms of the permeability, K. Perturbation-based SME formulations, on the other hand, have traditionally used a pressure, or head, equation written in terms of log-permeability, Y.

In MCS, we deal with individual realizations of the permeability field. In each realization, the permeability is represented as a discrete and discontinuous variable. The severity and nature of the discontinuities depend on the variance level and properties of the correlation structure. While Eqs. (1) and (2) are identical if K is a continuous variable, the results obtained from discrete forms that correspond to these two equations can be sensitive to the properties of the permeability field and the details of the discretization.

The simple discretization scheme employed to arrive at Eq. (18) leads to computational difficulties when applied to discontinuous permeability distributions. The matrix $\mathbf{Y}$ in Eq. (18) may not be diagonally dominant due to the way in which the terms involving the first derivative, such as $Y_{i+\frac{1}{2},j} - Y_{i-\frac{1}{2},j}$, are approximated. This problem is especially severe when the permeability variability is high and the correlation scales are small. Thus, use of the Y-based Eq. (18) for Monte Carlo simulation is not practical. This is why Monte Carlo simulations are usually performed using the K-based Eq. (7). To remove this discrepancy, one can apply a flux-continuous discretization scheme to the Y-based equations so that they are completely consistent with K-based MCS. That way, one retains all the benefits of a numerical Y-based SME formulation. The details of such an approach will be the subject of a subsequent paper.

3.6. Y-Based stochastic moment equations

Eq. (18) is the discrete form of Eq. (2). We use Eq. (18) as the starting point for developing a discrete form of the Y-based stochastic moment equations. Decomposing Y into a mean, $\langle Y \rangle$, and fluctuation, Y', substituting in Eq. (18), and averaging, we obtain a compact representation of the discrete mean-pressure equation

$$\langle \mathbf{Y} \rangle \langle \mathbf{P} \rangle + \langle \mathbf{Y}' \mathbf{P}' \rangle = 0. \tag{19}$$

Subtracting Eq. (19) from Eq. (18) yields the perturbation equation

$$\langle \mathbf{Y} \rangle \mathbf{P}' + \mathbf{Y}' \langle \mathbf{P} \rangle + \mathbf{Y}' \mathbf{P}' - \langle \mathbf{Y}' \mathbf{P}' \rangle = 0, \tag{20}$$

where $\langle \mathbf{Y} \rangle$ and $\langle \mathbf{Y}' \rangle$ are matrices representing the discretization of the mean and perturbation of log-permeability, respectively; $\langle \mathbf{P} \rangle$ and $\mathbf{P}'$ are vectors of the mean and perturbation of pressure. To obtain the equation for C_{YP}, we multiply Eq. (20) by Y' at a different location and take expectation, which gives

$$\langle \mathbf{Y} \rangle C_{YP} + \mathbf{C_{YY}} \langle \mathbf{P} \rangle + \langle Y' \mathbf{Y}' \mathbf{P}' \rangle = 0, \tag{21}$$

where $C_{YP} = \langle Y' \mathbf{P}' \rangle$ is the cross-covariance vector of log-permeability and pressure. $\mathbf{C_{YY}}$ is the matrix representing the derivative of the covariance of Y' with every point in the domain $\mathbf{Y}'$. Similarly, we multiply Eq. (20) by P' at a different location and average to obtain

$$\langle \mathbf{Y} \rangle C_{PP} + \mathbf{C_{PY}} \langle \mathbf{P} \rangle + \langle P' \mathbf{Y}' \mathbf{P}' \rangle = 0, \tag{22}$$

where $\mathbf{C_{PY}}$ is the matrix of the discretized derivative of the cross-covariance of P and Y.

Eqs. (21) and (22) are the discrete moment equations of pressure that correspond to the following equations in (continuous) differential form:

$$\frac{\partial^2 C_P(\mathbf{x}, \boldsymbol{\chi})}{\partial x_i^2} + \frac{\partial C_P(\mathbf{x}, \boldsymbol{\chi})}{\partial x_i} \frac{\partial \langle Y(\mathbf{x}) \rangle}{\partial x_i} + \frac{\partial C_{PY}(\mathbf{x}, \boldsymbol{\chi})}{\partial x_i} \frac{\partial \langle P(\mathbf{x}) \rangle}{\partial x_i} + \left\langle P'(\boldsymbol{\chi}) \frac{\partial Y'(\mathbf{x})}{\partial x_i} \frac{\partial P'(\mathbf{x})}{\partial x_i} \right\rangle = 0 \tag{23}$$

and

$$\frac{\partial^2 C_{YP}(\mathbf{x}, \boldsymbol{\chi})}{\partial \chi_i^2} + \frac{\partial C_{YP}(\mathbf{x}, \boldsymbol{\chi})}{\partial \chi_i} \frac{\partial \langle Y(\boldsymbol{\chi}) \rangle}{\partial \chi_i} + \frac{\partial C_{YY}(\mathbf{x}, \boldsymbol{\chi})}{\partial \chi_i} \frac{\partial \langle P(\boldsymbol{\chi}) \rangle}{\partial \chi_i} + \left\langle Y'(\mathbf{x}) \frac{\partial Y'(\boldsymbol{\chi})}{\partial \chi_i} \frac{\partial P'(\boldsymbol{\chi})}{\partial \chi_i} \right\rangle = 0, \tag{24}$$

where $C_{YP}(\mathbf{x}, \boldsymbol{\chi}) = \langle Y'(\mathbf{x}) P'(\boldsymbol{\chi}) \rangle$ and $C_{PP}(\mathbf{x}, \boldsymbol{\chi}) = \langle P'(\mathbf{x}) P'(\boldsymbol{\chi}) \rangle$. Here, $\mathbf{x}$ represents any spatial location in the two-dimensional domain, and $\boldsymbol{\chi}$ is a reference point. In the above equations, summation over the number of dimensions is implied. Comparison of Eqs. (21) and (22) with (23) and (24) indicates that $\langle Y' \mathbf{Y}' \mathbf{P}' \rangle$ and $\langle P' \mathbf{Y}' \mathbf{P}' \rangle$ are the discrete forms of

$$\langle Y'(\mathbf{x}) \frac{\partial Y'(\boldsymbol{\chi})}{\partial \chi_i} \frac{\partial P'(\boldsymbol{\chi})}{\partial \chi_i} \rangle \quad \text{and} \quad \langle P'(\boldsymbol{\chi}) \frac{\partial Y'(\mathbf{x})}{\partial x_i} \frac{\partial P'(\mathbf{x})}{\partial x_i} \rangle,$$

respectively.

We must first close Eqs. (23) and (24) before we can attempt to solve them. One particular closure approximation commonly used in low-order stochastic analysis is to discard the higher-order moments. For example, in the equations governing the second moments, we drop terms that depend on the third moments, leading to

$$\frac{\partial^2 C_P(\mathbf{x}, \boldsymbol{\chi})}{\partial x_i^2} + \frac{\partial C_P(\mathbf{x}, \boldsymbol{\chi})}{\partial x_i} \frac{\partial \langle Y(\mathbf{x}) \rangle}{\partial x_i} + \frac{\partial C_{PY}(\mathbf{x}, \boldsymbol{\chi})}{\partial x_i} \frac{\partial \langle P(\mathbf{x}) \rangle}{\partial x_i} = 0 \tag{25}$$

and

$$\frac{\partial^2 C_{YP}(\mathbf{x}, \boldsymbol{\chi})}{\partial \chi_i^2} + \frac{\partial C_{YP}(\mathbf{x}, \boldsymbol{\chi})}{\partial \chi_i} \frac{\partial \langle Y(\boldsymbol{\chi}) \rangle}{\partial \chi_i} + \frac{\partial C_{YY}(\mathbf{x}, \boldsymbol{\chi})}{\partial \chi_i} \frac{\partial \langle P(\boldsymbol{\chi}) \rangle}{\partial \chi_i} = 0. \tag{26}$$

Eqs. (25) and (26) are identical to the first-order (in terms of $\sigma^2_{\ln K}$) equations governing the second pressure moments obtained via a formal perturbation expansion (Eqs. (8) and (9) of [29]). The compact discrete forms that correspond to these equations are

$$\begin{aligned} \langle \mathbf{Y} \rangle C_{PP} + \mathbf{C_{PY}} \langle \mathbf{P} \rangle = 0, \\ \langle \mathbf{Y} \rangle C_{YP} + \mathbf{C_{YY}} \langle \mathbf{P} \rangle = 0. \end{aligned} \tag{27}$$

Comparison of Eqs. (23) and (24) with (25) and (26) shows that the missing terms are two triplets. These triplets, which are to infinite-order in $\sigma_{\ln K}$, can be computed with the help of MCS results. That way, we quantify the exact difference between low-order SME approximations and the full solution.

4. Results and discussion

4.1. K-Based MCS vs. K-based SME

The full discrete SME equations, Eqs. (10) and (12), help us to identify the terms that are dropped in order to obtain LOSME approximations. Using our detailed MCS results, we compute all the terms that appear in Eqs. (10) and (12). The "reconstruction procedure" to obtain the full discrete K-based SME solution is:

1. Using the MCS results, compute $\langle \mathbf{K}'\mathbf{P}' \rangle$.
2. Solve Eq. (10) for the mean pressure, $\langle \mathbf{P} \rangle$, which should be identical to the mean pressure obtained from MCS.
3. Calculate $\langle K'\mathbf{K}' \rangle$ from the actual ensemble of the generated realizations.
4. Compute $\langle K'\mathbf{K}'\mathbf{P}' \rangle$ from MCS, and solve the second equation of (12) for C_{KP}.
5. Calculate $\langle P'\mathbf{K}'\mathbf{P}' \rangle$ from MCS, and solve the first moment equation in (12) for the pressure covariance, C_{PP}. This C_{PP} is identical to that computed directly with MCS.

Note that step 3 is used to ensure complete consistency between the K-based SME formulation and MCS in terms of the statistics of the log-permeability field. With this procedure, we isolate the contributions of each term that appears in Eqs. (10) and (12). As a result, we should be able to achieve an exact match between MCS and the full discrete form of the K-based SME for any input variance or correlation scale. This gives us a unique opportunity to examine the effects of truncating each of these terms and determine the validity range of the approximate SME approach.

The approximate low-order, K-based SME approach is equivalent to the following steps: (1) solve for the mean pressure using Eq. (10) without the $\langle \mathbf{K}'\mathbf{P}' \rangle$ term, then (2) solve Eq. (13), (3) compute the correction term $\langle \mathbf{K}'\mathbf{P}' \rangle$ from the solution of Eq. (13), and (4) apply it to the mean-pressure approximation. We refer to this procedure as the "truncated" K-based SME solution, or simply the SME solution. The K-based SME solution procedure just described is analogous to the first-order Adomian decomposition approach, in which, as summarized by Zhang [30], the statistical moments of pressure are derived directly from Eq. (1), i.e., in K-based form, instead of Eq. (2). We refer to adding the contributions of the triplet moments $\langle K'\mathbf{K}'\mathbf{P}' \rangle$ and $\langle P'\mathbf{K}'\mathbf{P}' \rangle$ to the truncated SME solution as the "reconstructed solution". If the discretization and numerical implementation of SME and MCS are consistent, the reconstructed solution should reproduce the direct results obtained from MCS.

We resort to a graphical representation of the results, and we use the following labels in the figures. "MC" refers to the full MCS solution; "SME" stands for the "truncated" SME solution; "SME + $\langle P'\mathbf{K}'\mathbf{P}' \rangle$" describes the effect of dropping C_{KKP}; "SME + $\langle K'\mathbf{K}'\mathbf{P}' \rangle$" considers the effect of dropping C_{PKP}. Finally, SME + $\langle P'\mathbf{K}'\mathbf{P}' \rangle$ + $\langle K'\mathbf{K}'\mathbf{P}' \rangle$ refers to the fully reconstructed solution.

Our computations, which span a wide parameter range, indicate that high-order terms have a negligible effect on the mean pressure, and that low-order SME solutions are very accurate. This is an important finding because first-order SME approximations of the mean is no more expensive than solving the flow equation for one realization in an MCS procedure. The fact that the low-order SME mean is both robust and computationally affordable suggests that such computation should be performed as part of normal practice.

Figs. 5–7 show the pressure variance along the line $y = L/2$. Each of these figures is for a particular value of σ_Y^2. Namely, σ_Y^2 of 0.5, 1, and 3. In each figure, we show solution for λ_Y/L of 0.1 and 0.05. The MCS solutions, which we take as a reference, in Figs. 5–7 indicate that the overall level of pressure variance in the domain increases with σ_Y^2. The curves are nearly symmetric, and the maximum value occurs near the center of the domain. Because Dirichlet boundary conditions are used, the variance at both ends is zero.

Figs. 5–7 also indicate that compared to MCS, the SME solutions overestimate the level of pressure variance everywhere in the domain. Moreover, these figures indicate clearly that for a given λ_Y/L, the discrepancy between MCS and SME increases with σ_Y^2. In Fig. 5, which is for $\sigma_Y^2 = 0.5$, the maximum difference between SME and MCS is less than 20%. Thus, for this case, K-based SME appears to be a reasonable approximation. However, when the variance is as high as three as shown in Fig. 7, the K-based SME predictions overestimate the pressure variance by as much as 100%.

Figs. 5–7 show that the "reconstructed solution" is indeed equivalent to the MCS solution, which is a reassuring fact. From Figs. 5–7, we also see that the effect of the triplet terms increases as σ_Y^2 increases. In the uniform mean flow case, which is the subject of this paper, we find that the two triplet moments, namely, C_{PKP} and C_{KKP} appear to carry opposite signs. However, for a given σ_Y^2, C_{KKP} is consistently much

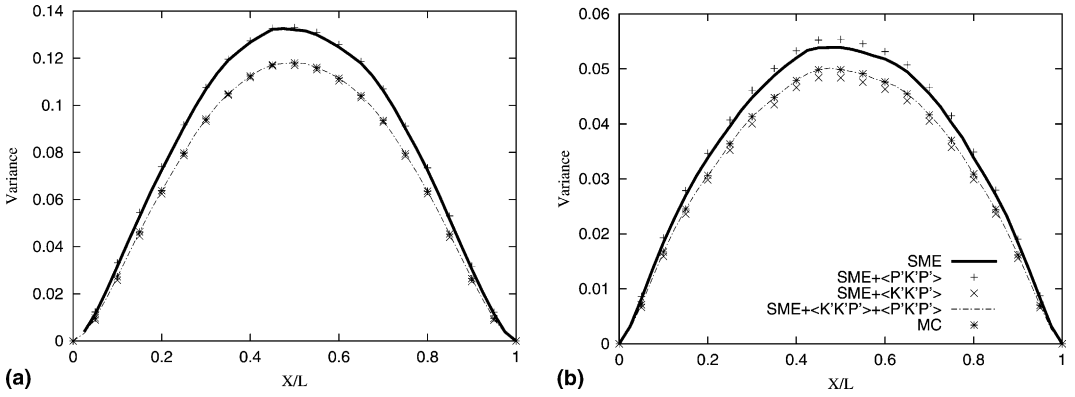

Fig. 5. The effect of dropped terms on the pressure variance prediction along the x direction at $y = L/2$, using K-based SME for uniform mean flow with $\sigma_{\ln k}^2 = .5$. (a) $\lambda_Y/L = 0.1$ and (b) $\lambda_Y/L = 0.05$.

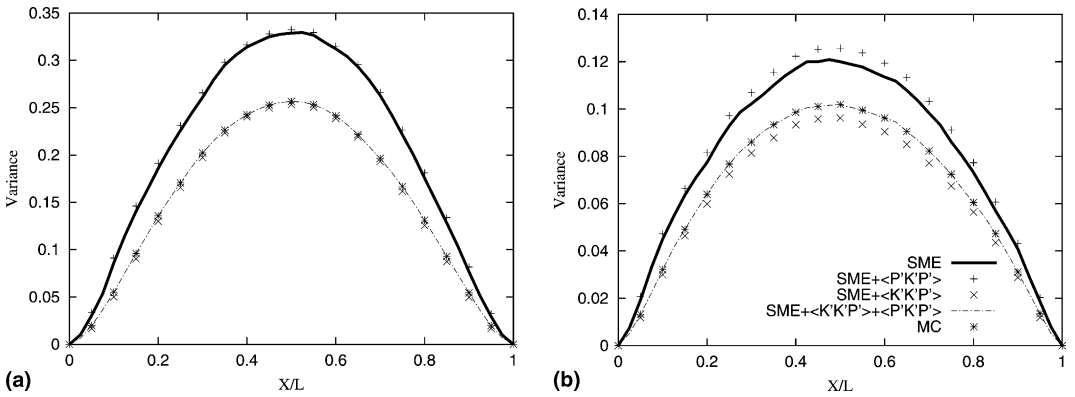

Fig. 6. The effect of dropped terms on pressure variance prediction along the x direction at $y = L/2$, using K-based SME for uniform mean flow with $\sigma_{\ln k}^2 = 1$. (a) $\lambda_Y/L = 0.1$; (b) $\lambda_Y/L = 0.05$.

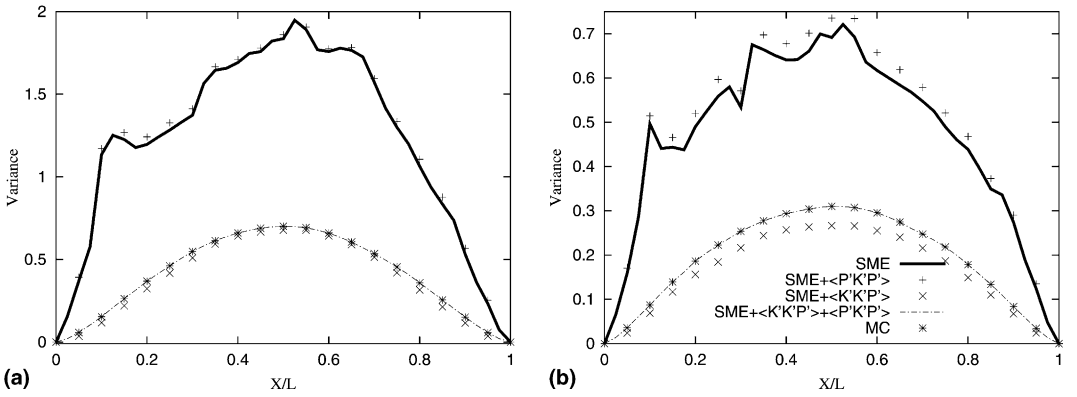

Fig. 7. The effect of dropped terms on pressure variance prediction along the x direction at $y = L/2$, using K-based SME for uniform mean flow with $\sigma^2_{\ln k} = 3$. (a) $\lambda_Y/L = 0.1$; (b) $\lambda_Y/L = 0.05$.

larger than C_{PKP}. These results highlight the importance of the triplet moment terms, especially C_{KKP}, when $\sigma^2_Y > 1$. Thus, an effort directed at improving K-based SME predictions should probably focus on accounting for the influence of C_{KKP}. Further examination of Figs. 5–7 indicates that for a given σ^2_Y, C_{PKP} appears to be more important when the integral scale of permeability is smaller. This is an interesting observation that requires further analysis. Figs. 5–7 indicate clearly that the truncated K-based SME approach is inadequate for providing uncertainty estimates of flow-related quantities when $\sigma^2_Y \geqslant 1$.

4.2. K-Based MCS vs. Y-based SME

4.2.1. Discrepancy between K-based and Y-based equations

Before we present detailed comparisons of K-based MCS with Y-based SME, we discuss issues related to the discrete forms of the equations.

In deriving the Y-based equation, Eq. (2), from Eq. (1), we implicitly assume that K is a continuous variable. However, when a discrete representation of the permeability field is employed, as in MCS, the permeability can be very discontinuous. In cases of spatially variable permeability, the expression $\partial K/K\partial x = \partial Y/\partial x$ is only valid at the infinitesimal scale. The way that $\partial K/K\partial x$ and $\partial Y/\partial x$ are usually discretized is the cause of the numerical discrepancy. To our knowledge, this problem has not been reported in the literature. We illustrate this issue using the one-dimensional pressure equation as an example.

Interior nodes. The K-based one-dimensional pressure equation for an interior node, or gridblock, is

$$K_{i+\frac{1}{2}}P_{i+1} + K_{i-\frac{1}{2}}P_{i-1} - \left(K_{i+\frac{1}{2}} + K_{i-\frac{1}{2}}\right)P_i = 0. \tag{28}$$

Rearranging the above equation yields

$$\frac{K_{i+\frac{1}{2}} - K_{i-\frac{1}{2}}}{K_{i+\frac{1}{2}} + K_{i-\frac{1}{2}}}[P_{i+1} - P_{i-1}] + P_{i+1} + P_{i-1} - 2P_i = 0, \tag{29}$$

and replacing K_i by e^{Y_i}, we get

$$\frac{e^{Y_{i+\frac{1}{2}}} - e^{Y_{i-\frac{1}{2}}}}{e^{Y_{i+\frac{1}{2}}} + e^{Y_{i-\frac{1}{2}}}}[P_{i+1} - P_{i-1}] + P_{i+1} + P_{i-1} - 2P_i = 0. \tag{30}$$

Multiplying the numerator and denominator of the first term by $e^{-Y_{i-\frac{1}{2}}}$ gives

$$\frac{e^{Y_{i+\frac{1}{2}}-Y_{i-\frac{1}{2}}}-1}{e^{Y_{i+\frac{1}{2}}-Y_{i-\frac{1}{2}}}+1}[P_{i+1}-P_{i-1}]+P_{i+1}+P_{i-1}-2P_i=0. \tag{31}$$

When the difference, $Y_{i+\frac{1}{2}}-Y_{i-\frac{1}{2}}$, is sufficiently small, the expression becomes

$$\begin{aligned} &e^{Y_{i+\frac{1}{2}}-Y_{i-\frac{1}{2}}}-1\approx Y_{i+\frac{1}{2}}-Y_{i-\frac{1}{2}},\\ &e^{Y_{i+\frac{1}{2}}-Y_{i-\frac{1}{2}}}+1\approx 2, \end{aligned} \tag{32}$$

and the K-based equation approaches the Y-based pressure equation. So that

$$\left(Y_{i+\frac{1}{2}}-Y_{i-\frac{1}{2}}\right)\frac{(P_{i+1}-P_{i-1})}{2}+P_{i+1}+P_{i-1}-2P_i\approx 0 \tag{33}$$

or

$$\frac{\Delta Y}{\Delta x}\frac{\Delta P}{\Delta x}+\frac{\Delta^2 P}{\Delta x^2}\approx 0. \tag{34}$$

This derivation reveals a source of difficulty in comparing K-based MCS and Y-based SME solutions. For the numerical comparisons to be strictly valid, the following condition must be satisfied: $|Y_{i+\frac{1}{2}}-Y_{i-\frac{1}{2}}|\ll 1$. We refer to this difference term as the model error, δ, which appears only when we compare K-based MC with Y-based SME. The model error, δ, is given by

$$\begin{aligned} \delta &= (Y\text{-based})-(K\text{-based})=\left(Y_{i+\frac{1}{2}}-Y_{i-\frac{1}{2}}\right)\frac{(P_{i+1}-P_{i-1})}{2}-\frac{e^{Y_{i+\frac{1}{2}}-Y_{i-\frac{1}{2}}}-1}{e^{Y_{i+\frac{1}{2}}-Y_{i-\frac{1}{2}}}+1}[P_{i+1}-P_{i-1}]\\ &=\frac{(P_{i+1}-P_{i-1})}{2}\left[Y_{i+\frac{1}{2}}-Y_{i-\frac{1}{2}}-\frac{2\left[e^{Y_{i+\frac{1}{2}}-Y_{i-\frac{1}{2}}}-1\right]}{e^{Y_{i+\frac{1}{2}}-Y_{i-\frac{1}{2}}}+1}\right]\\ &=\frac{(P_{i+1}-P_{i-1})}{2}\left[\frac{[Y_{i+\frac{1}{2}}-Y_{i-\frac{1}{2}}][e^{Y_{i+\frac{1}{2}}-Y_{i-\frac{1}{2}}}+1]-2[e^{Y_{i+\frac{1}{2}}-Y_{i-\frac{1}{2}}}-1]}{e^{Y_{i+\frac{1}{2}}-Y_{i-\frac{1}{2}}}+1}\right]\\ &=\frac{(P_{i+1}-P_{i-1})}{2}\left[\frac{\frac{1}{6}(Y_{i+\frac{1}{2}}-Y_{i-\frac{1}{2}})^3+\mathrm{O}[(Y_{i+\frac{1}{2}}-Y_{i-\frac{1}{2}})^4]}{e^{Y_{i+\frac{1}{2}}-Y_{i-\frac{1}{2}}}+1}\right]. \end{aligned} \tag{35}$$

This is the discretization error between the two methods for the simple one-dimensional pressure problem. As the equation indicates, the model error decreases as $|Y_{i+\frac{1}{2}}-Y_{i-\frac{1}{2}}|$ approaches zero.

For the two-dimensional case, the discrepancy between the discrete forms of the K-based and Y-based equations in the interior of the domain is

$$\begin{aligned} \delta &= (K\text{-based})-(Y\text{-based})\\ &=\left(F_{i+\frac{1}{2},j}-1\right)P_{i+1,j}-\left(1-F_{i-\frac{1}{2},j}\right)P_{i-1,j}+\left(F_{i,j+\frac{1}{2}}-1\right)P_{i,j+1}-\left(1-F_{i,j-\frac{1}{2}}\right)P_{i,j-1}\\ &\quad-\left(Y_{i+\frac{1}{2},j}-Y_{i+\frac{1}{2},j}\right)\frac{(P_{i+1,j}-P_{i-1,j})}{2}-\left(Y_{i,j+\frac{1}{2}}-Y_{i,j+\frac{1}{2}}\right)\frac{(P_{i,j+1}-P_{i,j-1})}{2}, \end{aligned} \tag{36}$$

where

$$F_{i+\frac{1}{2},j}=\frac{4K_{i+\frac{1}{2},j}}{\left(K_{i+\frac{1}{2},j}+K_{i-\frac{1}{2},j}+K_{i,j+\frac{1}{2}}+K_{i,j-\frac{1}{2}}\right)},\quad F_{i,j+\frac{1}{2},j}=\frac{4K_{i,j+\frac{1}{2}}}{\left(K_{i+\frac{1}{2},j}+K_{i-\frac{1}{2},j}+K_{i,j+\frac{1}{2}}+K_{i,j-\frac{1}{2}}\right)}.$$

Boundary cells. The second source of the discrepancy is due to the implementation of the boundary conditions. At the corners, the discretization is equivalent to setting the two terms $(\partial Y/\partial y)$ $(\partial P/\partial y)$ and $(\partial Y/\partial x)$ $(\partial P/\partial x)$ to zero. That is, at the corners the equation reduces to

$$\left(\frac{\partial^2 P}{\partial x^2}+\frac{\partial^2 P}{\partial y^2}\right)_{i,j}=0, \tag{37}$$

and for non-corner boundary nodes, we have

$$\left(\frac{\partial^2 P}{\partial x^2}+\frac{\partial^2 P}{\partial y^2}\right)_{i,j}+\left(\frac{\partial Y}{\partial x}\frac{\partial P}{\partial x}\right)_{i,j}=0\quad\text{or}\quad\left(\frac{\partial^2 P}{\partial x^2}+\frac{\partial^2 P}{\partial y^2}\right)_{i,j}+\left(\frac{\partial Y}{\partial y}\frac{\partial P}{\partial y}\right)_{i,j}=0. \tag{38}$$

Discretization of the K-based equation, on the other hand, is based on flux continuity at gridblock interfaces. As a result, the discrete equation accounts for the presence of variable permeability values. Inspection of Eqs. (6) and (17) reveals the differences more clearly. In the continuous case, the K-based Eq. (1) and Y-based Eq. (2) are equivalent. However, the discrete forms corresponding to Eqs. (1) and (2) are not identical.

4.2.2. Comparison between K-based MCS and Y-based SME

We analyze the Y-based SME formulation, again with the help of our extensive K-based MCS results. We follow the same procedure outlined previously except that we work with Eqs. (19), (21) and (22). Explicitly, the "reconstruction procedure" for the Y-based SME approach is:

1. Using the MCS results, compute $\langle \mathbf{Y}'\mathbf{P}'\rangle$.
2. Solve Eq. (19) for the mean pressure, $\langle \mathbf{P}\rangle$, which should be identical to the mean pressure obtained from MCS.
3. Calculate $\langle Y'\mathbf{Y}'\rangle$ from the ensemble of generated realizations.
4. Compute $\langle Y'\mathbf{Y}'\mathbf{P}'\rangle$ from MCS, and solve Eq. (21) for C_{YP}.
5. Calculate $\langle P'\mathbf{Y}'\mathbf{P}'\rangle$ from MCS, and solve Eq. (22) for C_{PP}.

We use labels similar to those used in Figs. 5–7, but with Y replacing K throughout. The new label "MERR" stands for "model error", which is computed using Eq. (36).

As reported for the K-based SME method, Y-based SME predictions of mean pressure are in excellent agreement with MCS even for domains with high input permeability variance and significant correlation lengths. We add here that the robustness of the mean pressure obtained from low-order SME solutions is observed for more complex flow settings (e.g. converging/diverging flow around wells) than the simple case of uniform mean flow studied here.

Figs. 8–11 show the distribution of pressure variance along the x direction at $y = L/2$ in the case of uniform mean flow. Figs. 8 and 9 show the results for different correlation lengths when $\sigma_Y^2 = 1$. Figs. 10 and 11 are similar, but with $\sigma_Y^2 = 3$. The dimensionless correlation scale, λ_Y/L, in these figures ranges from 0.1 to 0.5. Examination of the MCS results, which we take as reference, shown in Figs. 8–11 indicates that for a particular correlation length, the variance of pressure throughout the domain increases with σ_Y^2. The variance of the response variable, pressure, is a measure of the uncertainty associated with predictions of the pressure distribution in the area of interest. These results imply that as the input variance, σ_Y^2, increases, the level of uncertainty in the obtained response, pressure in this case, increases.

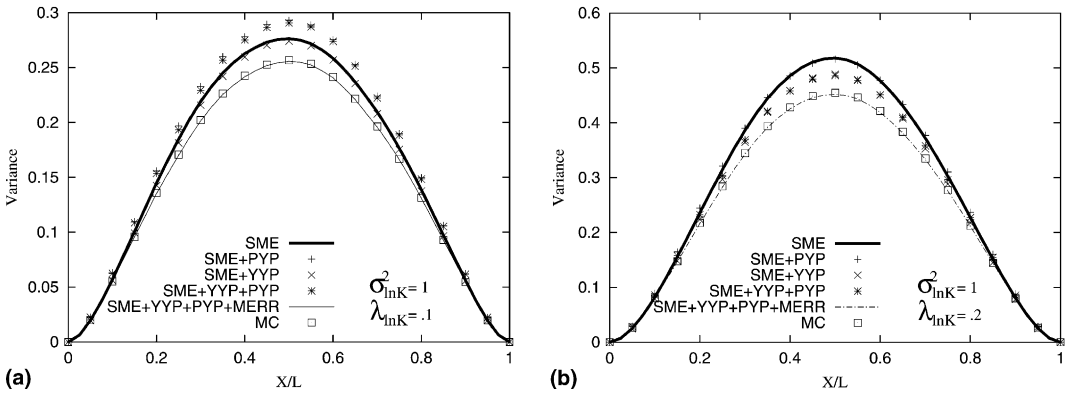

Fig. 8. The effect of dropped terms on pressure variance prediction along the x direction at $y = L/2$, using Y-based SME for uniform mean flow with $\sigma^2_{\ln k} = 1$. (a) $\lambda_Y/L = 0.1$; (b) $\lambda_Y/L = 0.2$.

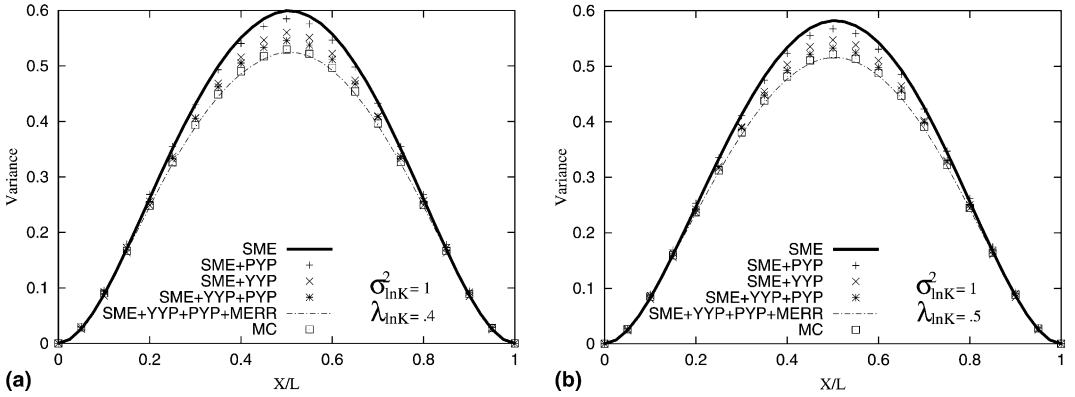

Fig. 9. The effect of dropped terms on pressure variance prediction along the x direction at $y = L/2$, using Y-based SME for uniform mean flow with $\sigma^2_{\ln k} = 1$. (a) $\lambda_Y/L = 0.4$; (b) $\lambda_Y/L = 0.5$.

Note that the maximum pressure variance is significantly smaller than the variance level of log-permeability. This attenuation of the statistical moments of the dependent variable compared to the input variance is an important characteristic of the flow problem [16,24], which deserves detailed analysis for heterogeneity models and flow settings of practical interest [32]. Examination of the MCS solutions of Fig. 8 indicates that for a domain of given size, the overall level of pressure variance increases significantly as the correlation length increases from 0.1 to 0.2. A similar behavior is observed for the $\sigma^2_Y = 3$ case of Fig. 10. This strong sensitivity of the second moment predictions to the correlation scale in this range has also been observed for radial flow in a bounded heterogeneous aquifer [25]. Increasing the correlation scale further, see Fig. 9, does not appear to change the overall response significantly. Similar behavior is also observed when $\sigma^2_Y = 3$ as shown in Figs. 10 and 11.

The results in Fig. 8(a), where $\sigma^2_Y = 1$ and $\lambda_Y/L = 0.1$, suggest that predictions of pressure variance obtained from the "truncated" Y-based SME solution are in close agreement with those predicted by Monte Carlo simulation. This result is consistent with the large body of published work in subsurface hydrology. Recall that our "truncated" Y-based SME approach is quite similar to the approximate moment analysis of Zhang [29]. The only difference is that when we compute the second moments, we use a mean

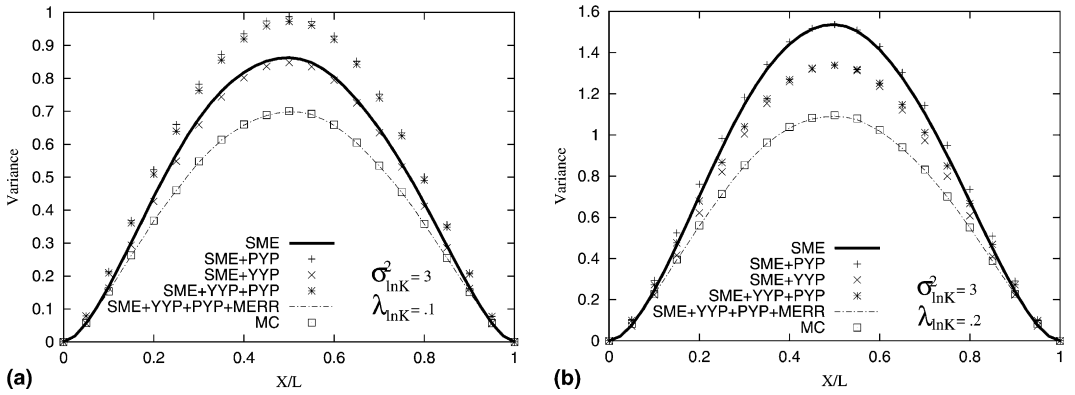

Fig. 10. The effect of dropped terms on pressure variance prediction along the x direction at $y = L/2$, using Y-based SME for uniform mean flow with $\sigma^2_{\ln k} = 3$. (a) $\lambda_Y/L = 0.1$; (b) $\lambda_Y/L = 0.2$.

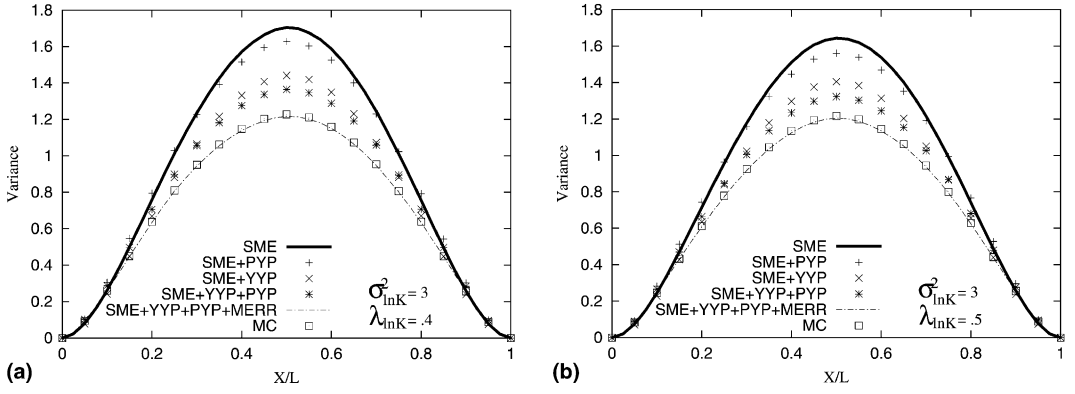

Fig. 11. The effect of dropped terms on pressure variance prediction along the x direction at $y = L/2$, using Y-based SME for uniform mean flow with $\sigma^2_{\ln k} = 3$. (a) $\lambda_Y/L = 0.4$; (b) $\lambda_Y/L = 0.5$.

pressure that is "corrected" by the doublet term $\langle \mathbf{Y}'\mathbf{P}' \rangle$ (see Eq. (19)). Zhang [29] used the first-order mean pressure in the second moment equations of pressure. For consistency, we verified that our code reproduces the solutions obtained from the SME analysis of zhang [29] when we use the mean pressure without the higher-order correction.

Fig. 8 also indicates that the discrepancy between MCS and SME increases slightly as the correlation scale increases. For this case, where $\sigma^2_Y = 1$, as the correlation length increases from 0.1 to 0.2, the maximum relative error in the SME predictions, with respect to the MCS solution, increases from 5% to 12%. For large correlation scales, see Fig. 9, the discrepancy between SME and MCS remains below 15%. This apparent increase in the difference between MCS and SME with correlation scale may be explained as follows. For a given domain size and σ^2_Y, as the correlation length increases, the spatial arrangement of permeability becomes more channel like, and the local flow becomes more non-uniform. This results in increased variability of the response variable, pressure and velocity for example. Under these conditions one expects the quality of an approximate perturbation-based SME solution to decrease somewhat.

Our experience from extensive comparisons between SME and MCS indicates that the SME solutions of first and second moments of pressure are robust for systems with $\sigma^2_Y \leqslant 1$. Thus, in this parameter space, the numerical Y-based SME approach, in which higher-order terms are neglected, especially triplets, provides

an elegant, yet powerful computational tool for assessment of prediction uncertainty. The discrepancy between predictions of the pressure's second moment obtained from SME and those from MCS increases as the variance of input log-permeability, σ_Y^2, exceeds one. For all the cases we studied, we find that compared to MCS, the first-order SME method overpredicts the magnitude of the pressure variance throughout the domain. This is an important observation that may prove quite useful in practice. The maximum error in the SME predictions relative to MCS when $\sigma_Y^2 = 3$ (see Figs. 10 and 11) is 17%, 38%, 39%, and 33% for $\lambda_Y/L = 0.1$, 0.2, 0.4, and 0.5, respectively. The evidence is clear that, overall, the quality of the Y-based SME predictions deteriorates with permeability variance and correlation length. However, given that SME formulations are usually based on truncated expansions in terms of a small parameter, that parameter being σ_Y^2, these results are very encouraging.

We now analyze the triplet terms. We begin with cases where $\lambda_Y/L \geqslant 0.2$. Figs. 8–11 show clearly that when $\lambda_Y/L \geqslant 0.2$, the effect of C_{YYP} is significantly larger than C_{PYP}. In fact, the effect of C_{PYP} is negligible for $\lambda_Y/L = 0.2$ (see Figs. 8(b) and 10(b)). From Figs. 9 and 11, in which $\lambda_Y/L = 0.4$ and 0.5, it is clear that the two triplet moment terms C_{PYP} and C_{YYP} have the same sign. These "corrections" combine to reduce the pressure variance levels predicted by the SME solutions, thus bringing them closer to the MCS results. Further study of Figs. 8–11 indicates that the triplet terms are more important in domains with larger variance. Detailed examination of the results indicates that the relative importance of the triplet terms in the Y-based formulation is much smaller than those in the K-based formulation. Specifically, while the C_{KKP} dominates the behavior of the second moment of pressure as σ_Y^2 increases, C_{YYP} does not.

Note, however, that in each of the plots of Figs. 8–11 the reconstructed solution, SME $+ \langle P'\mathbf{Y}'\mathbf{P}'\rangle + \langle Y'\mathbf{Y}'\mathbf{P}'\rangle$, does not reproduce the results from MCS. Recall that we did not encounter this problem when we compared K-based MCS with K-based SME. This discrepancy occurs when comparing Y-based SME with K-based MCS. As discussed in Section 4.2.1, we attribute the shortfall to differences in the treatment of the discrete forms of the governing equations, and we refer to it with the label "MERR" for model error.

The model error is an important component of the difference between SME and MCS solutions in Figs. 8–11. In fact, when the correlation length is small, the model error is dominant making it quite difficult to make any specific conclusions about the various terms in the equations. The presence of this "model error" complicates the analysis. This is especially the case here because we are interested in quantifying the impact of the various components that comprise the Y-based SME mathematical statement. From Figs. 8 and 9, which are for $\sigma_Y^2 = 1$, we see that the model error decreases as the correlation scale of log-permeability increases (i.e., permeability variability gets smoother locally). The same observation holds for Figs. 10 and 11, which are for σ_Y^2 of 3. Recall that we attribute the difference to the discontinuous nature of the discrete representation of the permeability field in a particular realization, and the manner in which the Y-based and K-based equations are approximated. As the correlation scale increases, one expects that, on average, the permeability values between adjacent gridblocks become more similar. Thus, the quality of finite-difference approximations like $Y_{i+\frac{1}{2},j} - Y_{i-\frac{1}{2},j}$ improves, and the model error decreases. Of course, in the limit of infinite correlation scale, the permeability is continuous and the discretizations of Y-based and K-based pressure equations become identical.

Consider Figs. 7(a) and 10(a), which are for the case $\sigma_Y^2 = 3$ and $\lambda_Y/L = 0.1$. While the errors of the K-based SME predictions of Fig. 7(a) render the method completely inadequate, the Y-based SME results of Fig. 10(a) provide a reasonable approximation with an error, measured relative to MCS, that does not exceed 17%. Our computational experience indicates that the Y-based formulation yields much better approximations of the pressure variance than a K-based approach. Note that both formulations yield accurate predictions of the mean pressure. Detailed analysis of the statistical moment behavior in the parameter space described in Table 1 provides compelling evidence that a Y-based SME formulation is superior to a K-based SME approach. This is particularly true when the focus is not only on computing the mean response, but also on quantifying the uncertainty associated with the flow predictions.

The superiority of the Y-based formulation is largely due to the fact that for systems with large variance, the contribution of C_{KKP} to the pressure variance is quite large while that of C_{YYP} is much smaller. As mentioned earlier, the (truncated) K-based moment equations are analogous to the (continuous) first-order moment equations derived with the Adomian decomposition approach. Zhang [30] shows that these truncated K-based equations can be formally derived using a perturbation expansion in terms of $\sigma_K/\langle K\rangle$. On the other hand, the first-order Y-based SME equations are obtained from a perturbation expansion where the small parameter is σ_Y. Thus, in a perturbation expansion, the third moment $\langle K'\mathbf{K}'\mathbf{P}'\rangle$ appears as a term of order $(\sigma_K/\langle K\rangle)^3$, while the third moment $\langle Y'\mathbf{Y}'\mathbf{P}'\rangle$ is of order σ_Y^3. When K is log-normally distributed, the following relation holds:

$$\sigma_Y^2 = \ln\left[1 + \left(\frac{\sigma_K}{\langle K\rangle}\right)^2\right]. \tag{39}$$

For small σ_Y (e.g., $\leqslant 0.4$), $\sigma_K/\langle K\rangle \approx \sigma_Y$ we may expect the two perturbation-based approaches to work equally well. For large σ_Y, we have $\sigma_K/\langle K\rangle \gg \sigma_Y$, for $\sigma_Y = 1.0$; $\sigma_K/\langle K\rangle = 1.31$, for $\sigma_Y = 1.73$; $\sigma_K/\langle K\rangle = 4.37$, for $\sigma_Y = 2.0$; $\sigma_K/\langle K\rangle = 7.32$. It is thus seen that the parameter σ_y is still relatively small when $\sigma_K/\langle K\rangle$ is already quite large. This may help explain the superior performance of a Y-based perturbation-based formulation over a K-based one when both are truncated at low-order [30].

5. Summary and conclusions

There is enormous interest in quantifying the uncertainty associated with predictions of flow and transport in porous media due to incomplete knowledge of the formation properties. The SME method is a direct approach for making predictions and providing a measure of the predictive reliability of these predictions. The recent developments toward a more general numerical solution framework for approximate SME approaches are very encouraging. Natural formations of interest often exhibit high levels of permeability variability and large spatial correlation scales. This class of porous media is of special interest here because of its importance in underground resources, such as oil and water reserves. Several investigators have indicated that approximate SME methods may indeed be applicable for such systems. This parameter space is significantly larger than what is expected based on theoretical considerations. The central question of the paper is the validity range of perturbation-based, low-order, SME methods for flow in heterogeneous porous media. In particular, the statistical moments of pressure for incompressible flow in two dimensions were the focus of this study.

We mapped out the behavior in the parameter space of interest, and we analyzed the character and magnitude of the errors that contribute to the discrepancy between truncated (low-order) SME solutions and MCS. All the MCS results reported here employ 9000 high-resolution realizations. The variance of log-permeability, σ_Y^2, ranged from 0.5 to 3.0 and correlation length (normalized by domain length) from 0.05 to 0.5. The errors are mainly due to terms that are usually dropped, or truncated, in the process of the developing low-order approximations. However, we also find that details of the numerical schemes employed are important.

We conclude with a list of the important findings of this study:

1. First-order estimates of the first moment of pressure are very robust. High-order corrections to the first moment are small even for systems with large log-permeability variance and long correlation scales (e.g. $\sigma_Y^2 = 3$ and $\lambda_Y/L = 0.5$). Both the Y-based and K-based approximate SME formulations give reliable estimates of the mean-pressure response.
2. Thousands of realizations are required to stabilize the second moments of pressure. Consistent with previous investigations of other flow-related quantities, we find that the adequate size of the ensemble tends to increase with both σ_Y^2 and λ_Y.

3. For the cases we studied here, we find that compared to MCS, the truncated Y-based SME method overpredicts the magnitude of the pressure variance. This is an important observation that may prove quite useful in practice. The discrepancy increases with the level of permeability variability and correlation length. The mismatch between MCS and SME is largely due to two triplet terms, which are mixed moments of pressure and permeability or log-permeability.
4. When the correlation scale is larger than 0.1 relative to the size of the domain, the contribution of C_{YYP} is larger than C_{PYP}. Similar, but more pronounced behaviors are observed for the K-based approach.
5. A Y-based SME formulation is superior to a K-based approach for predictions of the second moment of pressure. While the Y-based SME method produces reasonable approximations of second moments even for $\sigma_Y^2 = 3$, the truncated terms in K-based SME approximations, C_{KKP} in particular, are too important rendering the low-order K-based approach inadequate.
6. When comparing Y-based SME to K-based MCS, it is important to account for the differences in the details of the discretization methods, which we refer to as "model error". It is only after considering the model error that the reconstructed Y-based moment equation solution matches the Monte Carlo results exactly.

References

[1] R. Ababou, D. McLaughlin, L.W. Gelhar, A.F.B. Tompson, Numerical simulation of three-dimensional saturated flow in randomly heterogeneous porous media, Transport Porous Media 4 (1989) 549–565.
[2] K. Aziz, A. Settari, Petroleum Reservoir Simulation, Elsevier Applied Science Publishers, New York, 1979.
[3] A. Bellin, P. Salandin, A. Rinaldo, Simulation of dispersion in heterogeneous porous formations: statistics first-order theories, convergence of computations, Water Resour. Res. 28 (9) (1992) 2211–2227.
[4] A. Bellin, Y. Rubin, A. Rinaldo, Eulerian–Lagrangian approach for modeling of flow and transport in heterogeneous geological formations, Water Resour. Res. 30 (11) (1994) 2913–2924.
[5] A. Bellin, Y. Rubin, A new random number generator for correlated properties, Stochastic Hydrol. Hydraul. 10 (4) (1996).
[6] J.H. Cushman, The Physics of Fluids in Hierarchical Porous Media: Angstroms to Miles, Kluwer Academic Publishers, Norwell, MA, 1997.
[7] G. Dagan, Stochastic modeling of groundwater flow by unconditional and conditional probabilities. 1. Conditional simulation and the direct problem, Water Resour. Res. 18 (4) (1982) 813–833.
[8] G. Dagan, Solute transport in heterogeneous porous formations, J. Fluid Mech. 145 (1984) 151–177.
[9] G. Dagan, Flow and Transport in Porous Formations, Springer, New York, 1989, 465pp.
[10] J.P. Delhomme, Spatial variability and uncertainty in groundwater flow parameters: a geostatistical approach, Water Resour. Res. 15 (2) (1979) 269–280.
[11] F.-W. Deng, J.H. Cushman, On higher-order corrections to the flow velocity covariance tensor, Water Resour. Res. 31 (7) (1995) 1659–1672.
[12] C.V. Deutsch, A.G. Journel, GSLIB: Geostatistical Software Library and User's Guide, second ed., Oxford University Press, New York, 1998.
[13] M.D. Dettinger, J.L. Wilson, First-order analysis of uncertainty in numerical models of groundwater: Part 1. Mathematical development, Water Resour. Res. 17 (1) (1981) 149–161.
[14] R.A. Freeze, A stochastic-conceptual analysis of one-dimensional groundwater flow in non-uniform, homogeneous media, Water Resour. Res. 11 (5) (1975) 725–741.
[15] L.W. Gelhar, C.L. Axness, Three-dimensional stochastic analysis of macrodispersion in aquifers, Water Resour. Res. 19 (1983) 161–180.
[16] L.W. Gelhar, Stochastic Subsurface Hydrology, Prentice-Hall, Englewood Cliffs, NJ, 1993.
[17] W.D. Graham, D.B. McLaughlin, Stochastic analysis of nonstationary subsurface solute transport, 1. Unconditional moments, Water Resour. Res. 25 (2) (1989) 215–232.
[18] W.D. Graham, D.B. McLaughlin, Stochastic analysis of nonstationary subsurface solute transport, 2. Conditional moments, Water Resour. Res. 25 (11) (1989) 2331–2355.
[19] A. Guadagnini, S.P. Neuman, Nonlocal and localized analyses of conditional mean steady state flow in bounded, randomly nonuniform domains 1. Theory and computational approach, Water Resour. Res. 35 (10) (1999) 2999–3018.
[20] A. Guadagnini, S.P. Neuman, Nonlocal and localized analyses of conditional mean steady state flow in bounded, randomly nonuniform domains 2. Computational examples, Water Resour. Res. 35 (10) (1999) 2999–3018.

[21] A.E. Hassan, J.H. Cushman, J.W. Delleur, A Monte Carlo assessment of Eulerian flow and transport perturbation models, Water Resour. Res. 34 (5) (1998) 1143–1163.
[22] R.J. Hoeksema, P.K. Kitanidis, Analysis of the spatial structure properties of selected aquifers, Water Resour. Res. 21 (4) (1985) 563–572.
[23] S.P. Neuman, C.L. Winter, C.M. Newman, Stochastic theory of field-scale Fickian dispersion in anisotropic porous media, Water Resour. Res. 23 (3) (1987) 453–466.
[24] H. Osnes, Stochastic analysis of head spatial variability in bounded rectangular heterogeneous aquifers, Water Resour. Res. 31 (12) (1995) 2981–2990.
[25] M. Riva, A. Guadagnini, S.P. Neuman, S. Franzetti, Radial flow in a bounded randomly heterogeneous aquifer, Transport Porous Media 45 (1) (2001) 139–193.
[26] Y. Rubin, Stochastic modeling of macrodispersion in heterogeneous media, Water Resour. Res. 26 (1) (1990) 133–142.
[27] H.A. Tchelepi, L.J. Durlofsky, W.H. Chen, A. Bernath, M.C.H. Chien, Practical use of scale up and parallel reservoir simulation technologies in field studies, SPE Reservoir Eval. Eng. 2 (4) (1999) 368–376.
[28] D.G. Zeitoun, C. Braester, A Neumann expansion approach to flow through heterogeneous formations, Stochastic Hydrol. Hydraul. 5 (1991) 207–226.
[29] D. Zhang, Numerical solutions to statistical moment equations of groundwater flow in nonstationary, bounded, heterogeneous media, Water Resour. Res. 34 (3) (1998) 529–538.
[30] D. Zhang, Stochastic Methods for Flow in Porous Media: Coping with Uncertainties, Academic Press, San Diego, CA, 2002, 350pp.
[31] D. Zhang, C.L. Winter, Moment-equation approach to single phase fluid flow in heterogeneous reservoirs, Soc. Petrol. Eng. J. 4 (2) (1999) 118–127.
[32] D. Zhang, L. Li, H.A. Tchelepi, Stochastic formulation for uncertainty assessment of two-phase flow in heterogeneous reservoirs, Soc. Petrol. Eng. J. 5 (1) (2000) 60–70.